First-principles calculations of an oxygen deficient Σ = 3(111)[10] grain boundary in strontium titanate

2002 J. Phys.: Condens. Matter 14 6455

(http://iopscience.iop.org/0953-8984/14/25/313)

INSTITUTE OF PHYSICS PUBLISHING JOURNAL OF PHYSICS: CONDENSED MATTER

J. Phys.: Condens. Matter **14** (2002) 6455–6467 PII: S0953-8984(02)28774-3

First-principles calculations of an oxygen deficient $\Sigma = 3$ (111) [10$\bar{1}$] grain boundary in strontium titanate

R Astala and P D Bristowe

Department of Materials Science and Metallurgy, University of Cambridge, Cambridge CB2 3QZ, UK

Received 30 August 2001, in final form 17 May 2002
Published 14 June 2002
Online at stacks.iop.org/JPhysCM/14/6455

Abstract

An oxygen vacancy in a $\Sigma = 3$ (111) [10$\bar{1}$] grain boundary (GB) in $SrTiO_3$ is modelled using DFT plane-wave pseudopotential methods. The formation energy of the vacancy in the boundary is found to depend on its charge state and on the electron chemical potential. There is a strong driving force for segregation when the vacancy is in the charge neutral state and this results in an electrostatic potential barrier at the GB. The vacancy is found to act as a donor and the GB becomes n-type. The defect induces small atomic relaxations in an otherwise highly ordered GB structure.

1. Introduction

Strontium titanate ($SrTiO_3$) is an electroceramic material with a large dielectric constant. At room temperature it has the cubic perovskite structure with a lattice parameter of 3.905 Å [1]. It is typically used in capacitor devices [2, 3] although recently it has been suggested as a possible gate dielectric in field effect transistors [4]. The electronic properties of $SrTiO_3$ can be modified by point defects, dopants and grain boundaries (GBs). Of the point defects, oxygen vacancies are particularly important since by controlling their concentration it is possible to alter the conductivity of the material and determine whether it is n- or p-type [5]. The oxygen vacancy has been identified as an effective donor and its properties have been studied using various computational methods including empirical, plane-wave pseudopotential and LMTO-ASA methods [6–10]. One study has shown that the vacancy is most likely to exist in a charge state of +2 [9]. GBs are also important defects since they are interfaces which act as regions of high electrical resistance and can be utilized in GB barrier layer capacitors. GBs are two-dimensional regions of the material which may exhibit changes in atomic coordination, non-stoichiometry and partially occupied atomic columns. Importantly, there have been experimental and theoretical studies, focusing mainly on high-angle [001] tilt boundaries [11–21], which conclude that some GBs contain vacant sites. The electrical properties of such boundaries have been studied and in one case it has been deduced that the formation of a potential barrier and pnp-type behaviour in the vicinity of the GB is specifically due to the

Table 1. The supercells used in the calculations.

Shape	Size (atoms)	Cell edge vectors (a_0)	Grain boundary separation (Å)
Hexagonal	30	$[10\bar{1}]$ $[\bar{1}10]$ 2[111]	6.9
	40	$[10\bar{1}]$ $[\bar{1}10]$ 8/3[111]	9.2
	60	$[10\bar{1}]$ $[\bar{1}10]$ 4[111]	13.6
	120	2$[10\bar{1}]$ 2$[\bar{1}10]$ 2[111]	6.9
Tetragonal	40	2[100] 2[010] 2[001]	—

presence of oxygen vacancies [20]. Other than this study, very little is known about the influence of vacancies on the electronic properties of interfaces in strontium titanate or the energetics of point defect segregation.

In this paper we investigate these properties by studying, using first-principles computational methods, a model GB system with and without oxygen vacancies. We have chosen the $\Sigma = 3$ (111) $[10\bar{1}]$ tilt boundary since it has been the subject of previous experimental and theoretical studies [22, 23]. It is also a twin boundary with relatively low interfacial energy and therefore should be commonly occurring in strontium titanate. The same boundary structure has been observed in $BaTiO_3$ and also modelled using first-principles methods [24]. The structure of the boundary is very similar in both materials. In $SrTiO_3$, high-resolution transmission electron microscopy suggests that the boundary is highly ordered, mirror symmetric, stoichiometric and has a small volume expansion. The theoretical studies confirm this and furthermore indicate that the boundary does not exhibit electrical activity. However, the effect of point defects on the structural and electronic properties was not examined in these studies. The geometry of the interface is such that the formation energy of the oxygen vacancy should differ from its value in the bulk. It is also of interest to determine whether the segregation of an oxygen vacancy to the boundary results in n-type electrical behaviour as it does for [001] tilt boundaries which have less ordered structures.

2. Grain boundary calculations

2.1. The grain boundary and vacancy models

To model the vacancies and the (111) GB, five different types of periodic supercell were constructed, four hexagonal and one tetragonal. The hexagonal cells were constructed to model the GB. Four different sizes were used (see table 1) to gauge the effect of supercell interactions on the results. In these cells, the basis vectors are expressed in the cubic system as $[10\bar{1}]$, $[\bar{1}10]$ and [111]. These systems are typically tall and narrow in the [111] direction. For example, the dimensions of the 60-atom hexagonal supercell are $4\sqrt{3}a_0$ along [111] and $\sqrt{2}a_0$ along $[10\bar{1}]$ and $[\bar{1}10]$, where a_0 is the lattice parameter of cubic $SrTiO_3$. The tetragonal cell was constructed to model the oxygen vacancy in the bulk crystal and was constructed from eight $SrTiO_3$ unit cells in a cubic arrangement, with a small deviation in its lattice parameters which breaks the ideal cubic symmetry. This model had 40 atoms.

The GBs were formed in the hexagonal supercells by cutting along a (111) plane and rotating one half of the crystal by 180° around the [111] axis. Therefore, because of the periodic boundary conditions, each supercell contained two equivalent (111) boundaries. The boundary configuration constructed this way is stoichiometric and highly ordered. Figure 1 shows the relaxed 60-atom stoichiometric GB model obtained after minimization of the total energy. There are, in fact, two distinct structural variants of the (111) boundary, one in which

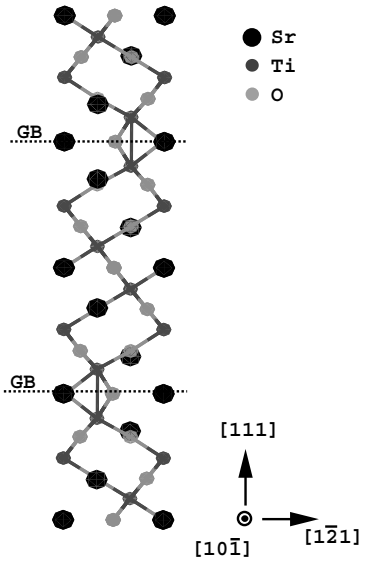

Figure 1. The atomic structure of the $\Sigma = 3$ (111) [10$\bar{1}$] GB in $SrTiO_3$ showing the relaxed 60-atom supercell geometry. The supercell contains two symmetry-related but equivalent GBs indicated by GB. Note the small dissociation of the Sr–O columns adjacent to the GB plane.

the boundary plane coincides with a Ti layer and another in which the boundary plane coincides with a Sr–O layer. In this work, only the Sr–O boundary is considered since empirical shell-model calculations find it to have a lower GB energy and this structure best matches the observations [22].

The GB vacancies were incorporated into the hexagonal supercells by removing a single oxygen atom from the core of one of the two GBs in the model. Since all of the oxygen atoms in the boundary core are equivalent due to the threefold rotational symmetry, the choice is arbitrary. In the 60-atom model this resulted in the removal of one-third of the oxygen atoms from the Sr–O boundary layer. Because of the periodic border conditions, the oxygen vacancy is then separated from its images in the neighbouring cells by $\approx\sqrt{2}a_0 = 5.6$ Å. In the 120-atom model the fraction of missing oxygen atoms is $1/12$ and the corresponding image separation is $2\sqrt{2}a_0 = 11.2$ Å. The larger model thus effectively allows the study of an isolated defect in the GB core although in this case the GBs are closer together than they are in the 60-atom model. The 30- and 40-atom models were used to check the convergence of the calculations with respect to GB separation. In all of these models the system was treated as charge neutral. However, it is known from previous work [9] that the oxygen vacancy prefers to exist in the +2 charge state in the bulk. Therefore, to probe the different charge states of the vacancy in the GB, a 119-atom model was constructed in which the supercell was charged in a +1 or +2 state. In order to determine the formation energies of these charged vacancies, appropriately charged bulk reference models were also constructed. In the bulk calculations where the supercell is tetragonal, the image separation of the vacancies is $2a_0 = 7.9$ Å. Previous calculations using the local spin density approximation have indicated that the image interactions for this sized supercell are negligible [9].

In a supercell calculation the energy of an oxygen vacancy in a charge state n can be written as

$$E_v = E^0_{v,n} - E^0_{bulk} + n\mu(\mathrm{e}) + \mu(\mathrm{O}) + \Delta E \tag{1}$$

where $E^0_{v,n}$ is the total energy of the supercell containing the vacancy and having a net charge of ne, E^0_{bulk} is the total energy of a defect-free supercell and μ(e) and μ(O) are the electron and oxygen chemical potentials. In addition, a uniform jellium background charge $-ne/V_c$, where V_c is the volume of the supercell, is used to compensate for the otherwise diverging interactions between charged periodic supercells [25]. The final term on the right-hand side of the equation is a correction for spurious interactions between periodic images. For a charged cubic supercell containing a point defect this correction can be given as [26]

$$\Delta E = -q\langle\Phi\rangle - \frac{\alpha q^2}{2\epsilon L} - \frac{2\pi q}{3\epsilon V_c}\int_\Omega \rho_1(\boldsymbol{r})\boldsymbol{r}^2\,\mathrm{d}\boldsymbol{r} + \frac{1}{2}\int_{\boldsymbol{r}'\notin\Omega}\int_{\boldsymbol{r}\in\Omega}\frac{\rho_1(\boldsymbol{r}')\rho_d(\boldsymbol{r})}{|\boldsymbol{r}'-\boldsymbol{r}|}\,\mathrm{d}\boldsymbol{r}'\,\mathrm{d}\boldsymbol{r}. \tag{2}$$

Here ρ_d is the local distortion of the bulk charge density induced by the defect and ρ_1 is ρ_d made neutral by subtracting a point charge from it. Ω denotes the supercell, L is the length of the supercell, ϵ is the dielectric constant and α is the Madelung constant. The $\langle\Phi\rangle$ term is the average bulk electrostatic potential and can be evaluated as

$$-q\langle\Phi\rangle = E^0_{bulk,-n} - E^0_{bulk}$$

where $E^0_{bulk,-n}$ is the total energy of the bulk supercell with net charge of $q = -ne$. All the other correction terms tend to zero as the supercell size increases. Since our earlier work [9] indicated that errors caused by image interactions are insignificant for $L = 7.9$ Å and the model sizes employed in this study are at least this size, we have only included the $q\langle\Phi\rangle$ correction term in the calculations.

To estimate the oxygen chemical potential μ(O), we calculated the energy of an isolated O_2 molecule in a supercell having the same dimensions as the tetragonal 40-atom model. This enabled the formation energy of the oxygen vacancy (V_O) to be estimated for the process in which oxygen ions diffuse into the atmosphere and recombine into O_2 molecules, i.e. $O_O \rightarrow V_O + \frac{1}{2}O_2$.

It is noted that the formation energies evaluated in this fashion are only valid at $T = 0$ K since no entropy contributions are taken into account. For a fuller thermodynamic treatment of vacancy formation energies in ordered compounds see [27]. Also, more complicated processes such as the formation of compensating cation vacancies or interstitials are not considered here since the work primarily focuses on the difference between formation energies in the bulk and in the GB. The formation energy of the vacancy at the GB can be calculated by simply replacing the $E^0_{v,n} - E^0_{bulk}$ terms in equation (1) by terms such as $E^0_{v,gb,n} - E^0_{gb}$ for the GB. Finally, the GB energy s is defined as

$$s = (E^0_{gb} - E^0_{bulk})/2A \tag{3}$$

where A is the surface area of the GB and the factor of $1/2$ accounts for the presence of two GBs in the supercell.

2.2. Computational methods

The calculations are based on density-functional theory [28] in the generalized gradient spin density approximation using the Perdew–Wang functional (GGS) and were performed using the CASTEP software[1]. The electron–ion interactions are described by Vanderbilt ultrasoft pseudopotentials [29] which are available with the software and define the number of valence electrons that are treated explicitly in the calculations. For Sr these are 4s, 4p and 5s states, for O 2s and 2p states and for Ti 3s, 3p, 3d and 4s states. The electron wavefunctions were expanded in plane waves and the electronic ground state was reached using a conjugate gradients algorithm [30]. Monkhorst–Pack meshes were used for the Brillouin zone sampling [31].

[1] CASTEP 3.9 and 4.2; CERIUS (Accelrys).

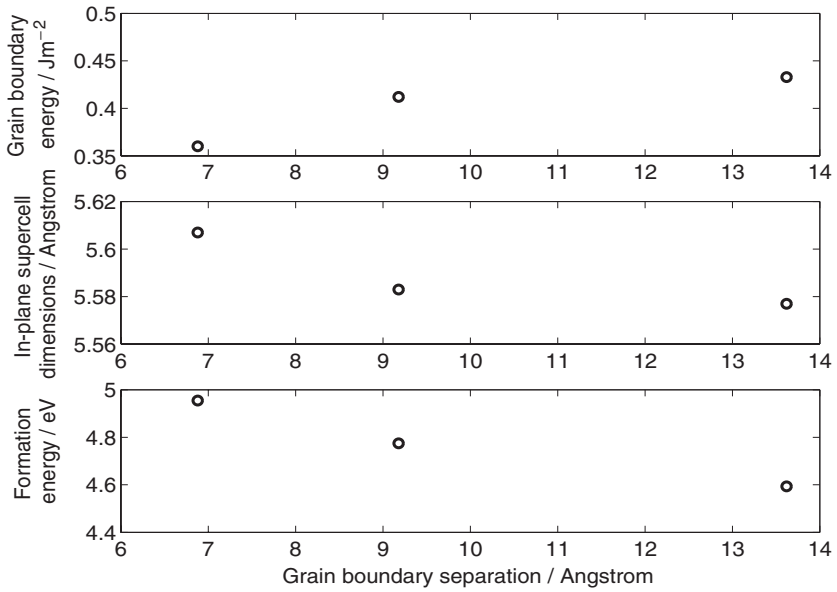

Figure 2. The convergence of GB energy, in-plane supercell dimension and vacancy formation energy as a function of GB separation in the 30-, 40- and 60-atom models.

The BFGS optimization method [30] was used to find the relaxed atomic structure of the GB. The 60-atom hexagonal and 40-atom tetragonal models were relaxed in two steps. First, a lower kinetic energy cut-off and k-point sampling density were used to speed up the initial stages of the calculation. Then, the space group symmetry of the structure was analysed and the structure constrained to that symmetry. This enabled a more accurate final relaxation to be performed using a larger kinetic energy cut-off and higher k-point density with symmetrized Monkhorst–Pack meshes. The atomic relaxations were found to be small and even the structures containing vacancies still possessed a significant degree of symmetry. This procedure permitted a considerable reduction in the absolute number of k-points. For the 60-atom stoichiometric models, a $3 \times 3 \times 1$ mesh was initially used together with a kinetic energy cut-off $E_c = 380$ eV. Then the accuracy was increased by using a $4 \times 4 \times 2$ mesh with $E_c = 400$ eV. For the 59-atom vacancy model, the same parameters were used except that the final mesh size was $4 \times 4 \times 1$. For the isolated oxygen vacancy in the tetragonal supercell a symmetrized $3 \times 3 \times 3$ mesh was used and the kinetic energy cut-off was 400 eV. For the 30- and 40-atom GB models with and without the vacancy a $4 \times 4 \times 2$ mesh with $E_c = 400$ eV was used. For the large 120- and 119-atom models, the Γ-point approximation with $E_c = 400$ eV was first employed. After the structure was relaxed a single point energy calculation was performed using a symmetrized $2 \times 2 \times 2$ mesh. No additional atomic relaxations were carried out due to the computationally intensive nature of these calculations. In most of the calculations the supercell angles were fixed. The partial densities of states (PDOSs), Mulliken charges and overlap populations were calculated for the relaxed 60-atom GB, vacancy and bulk systems using techniques based on projecting the Kohn–Sham plane wave eigenstates onto a linear combination of atomic orbitals basis set. Whilst the *absolute values* of the Mulliken charges depend on the basis set used, the Mulliken charge *differences* have significantly weaker basis set dependence and therefore they can be used to analyse charge transfer effects [32, 33].

3. Results

3.1. Stoichiometric grain boundaries

The relaxed stoichiometric $\Sigma = 3$ (111) GB structure was found to be highly ordered and mirror symmetric in agreement with the previous computational studies [22, 23]. The atomic structure obtained using the 60-atom model is presented in figure 1. In general the atomic displacements away from the starting geometrical configuration based on the coincidence site lattice were very small. The most significant displacements occurred normal to the boundary plane. In the 30- and 60-atom models the Ti plane nearest to the GB moved outwards by 0.21 and 0.19 Å, respectively. The second-nearest plane to the GB, which is a Sr–O plane, tended to dissociate into separate Sr and O planes. In the 30-atom model, the separation between these dissociated planes was found to be 0.32 Å with the Sr atoms closer to the boundary. In the 60-atom model this separation decreased to 0.07 Å indicating better agreement with the experimental HRTEM results where no separation was observed [22]. The relaxation of atoms in the plane of the GB was negligible. The displacements are very similar to those found for the same boundary in $BaTiO_3$ [24]. The calculated GB energies obtained using equation (3) as a function of system size are plotted in figure 2. The results show that the energies approach a limiting value as the distance between the two boundaries increases. Interestingly the boundary energy reduces for very small boundary separations (6.9 Å). However, for the largest boundary separation considered (13.8 Å, 60-atom model) the energy is considered to be sufficiently well converged. Figure 2 also shows how the in-plane supercell size and the formation energy of a charge neutral oxygen vacancy vary with boundary separation. Both of these quantities also show convergent behaviour. The GB energy calculated for the model with largest boundary separation was 0.42 J m^{-2} which is somewhat lower than a previously reported value of 0.52 J m^{-2} [23]. In addition to investigating the effect of boundary separation on boundary energy, we also studied the convergence of the energy with respect to k-point density. When the total energies of different bulk supercells were compared, it was found that the energy differences between $4 \times 4 \times 1$ and $4 \times 4 \times 2$ Monkhorst–Pack grids were negligible since the k-point density in the reciprocal [111] direction was large in all cases. Also the GB energies in the 30- and 120-atom models, where the boundary separation was the same (6.9 Å), were within 2% of one another.

In order to understand the electronic structure of the GB, the PDOSs were evaluated and a Mulliken population analysis was performed. The Mulliken charges on atoms for the bulk system, the stoichiometric GB and the GB containing a charge neutral oxygen vacancy are presented in table 2. For the stoichiometric GB, the Mulliken charges were found to be dependent on the distance of the atom from the GB plane. Comparison with the bulk values reveals some redistribution of valence charge. The Sr atoms, particularly those in the GB plane, gain valence charge whereas the O atoms in this plane and all of the Ti atoms lose valence charge. Away from the GB, i.e., in the sixth layer, the charges were found to approach the bulk values.

The calculated bandgap of the 60-atom bulk system was found to be 1.9 eV which is less than the experimental value of 3.2 eV [34]. However, this underestimation of the bandgap is expected when using density functional theory. For the 60-atom GB system the bandgap reduced slightly to 1.8 eV. The electron density of states of the stoichiometric GB structure was very similar to that of bulk $SrTiO_3$. Figure 3 shows the PDOS of this structure where it is seen that the highest valence band consists of O p states and the lowest conduction band consists of Ti d states and that these states are partially hybridized with each other, as expected. The Ti d–O p hybridization was further supported by the Mulliken population analysis which indicated

Table 2. Mulliken charges for bulk $SrTiO_3$, the stoichiometric 60-atom GB model and the GB model containing a charge neutral oxygen vacancy. The values are presented in units of elementary charge $|e|$. The location refers to the Sr–O and Ti atom layers parallel to (111) and to their distance from the GB. In the case of the non-stoichiometric GB, 'GB plane' refers to the GB containing the oxygen vacancy, whereas '2nd GB plane' refers to the second defect-free GB in the model.

		Mulliken charge (e)	
Atom	Location	Stoichiometric GB	GB with oxygen vacancy
Sr	GB plane	1.90	1.91
	2nd layer	1.93	1.93
	4th	1.97	1.96
	6th	1.97	1.96
	8th	1.97	1.96
	10th	1.93	1.92
	2nd GB plane	1.90	1.89
Sr	Bulk $SrTiO_3$	1.96	
Ti	1st layer	0.72	0.67
	3rd	0.75	0.72
	5th	0.71	0.65
	7th	0.71	0.68
	9th	0.75	0.71
	11th	0.72	0.70
Ti	Bulk $SrTiO_3$	0.69	
O	GB plane	−1.00	−0.92, −0.92
	2nd layer	−0.86	−0.81, −0.94, −0.94
	4th	−0.86	−0.91, −0.89, −0.89
	6th	−0.91	−0.89, −0.92, −0.92
	8th	−0.86	−0.87, −0.86, −0.86
	10th	−0.86	−0.87, −0.88, −0.88
	2nd GB plane	−1.00	−1.01, −1.02, −1.02
O	Bulk $SrTiO_3$	−0.89	

partial covalency of the Ti–O bonds. The overlap population was found to be 0.52 in the bulk structure and 0.49–0.56 in the GB structure. For the bond between the Ti atom adjacent to the GB plane and the O atom in the GB plane, the overlap population reduced to 0.38. The projection scheme worked well for the entire Mulliken population analysis, including the conduction band Ti d states, producing a spilling parameter of $<3\%$.

3.2. Grain boundaries with oxygen vacancies

Figure 2 illustrates the formation energy of the charge neutral vacancy in the GB as a function of boundary separation in the model. It shows reasonably convergent behaviour and for the model with the largest boundary separation the formation energy is found to be 4.59 eV. This compares with a value of 5.42 eV for the same vacancy in the bulk thus indicating a significant driving force for segregation. The bulk formation energy is somewhat lower than the value found in a previous study (6.67 eV) [9] probably because of the present use of the generalized gradient approximation which should treat both the isolated oxygen molecule and the occupied Ti d orbitals in the model containing the vacancy more accurately. The formation energy of the vacancy was also calculated at a position midway between the two GBs in the 59-atom model which had the largest boundary separation and found to be 5.00 eV. This result would suggest that part of the energy gain in segregating to the boundary is due to vacancy clustering

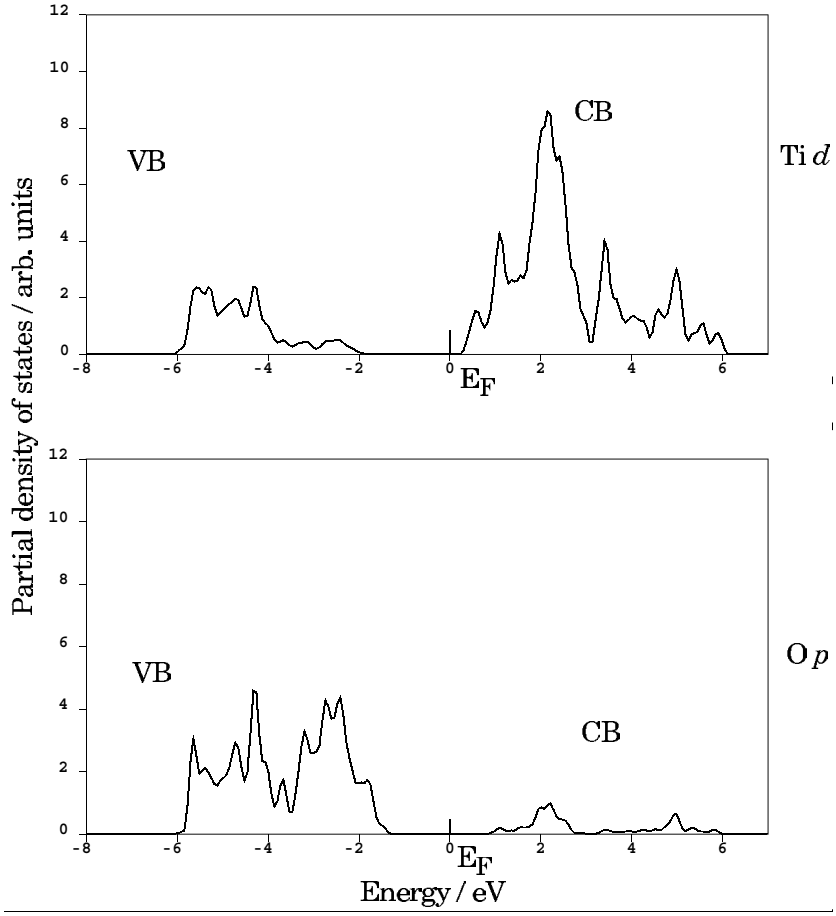

Figure 3. The PDOS for bulk $SrTiO_3$ obtained using a 60-atom supercell. For simplicity, only the Ti d states and O p states are shown. CB and VB denote the conduction and valence bands respectively.

caused by the periodic boundary conditions. To minimize the image interactions between neighbouring cells, the vacancy formation energy was calculated in the 119-atom model and was found to be 4.48 eV. This reinforces the earlier conclusion that oxygen vacancies will segregate to this boundary which should be a sink for these defects. All of these results apply to the oxygen vacancy in its charge neutral state. However, as shown in earlier work [9], the oxygen vacancy in the bulk prefers to have the +2 charge state. It is therefore important to consider whether charged vacancies also segregate to the boundaries.

To evaluate whether an oxygen vacancy in a non-neutral charge state still segregates to the GB, its formation energy in the +1 and +2 state was determined using the 119-atom model. The results are shown in figure 4 together with the corresponding energies for the bulk crystal using the 39-atom model. The values were determined using equation (1) and are shown as a function of electron chemical potential. The formation energies are linear in $\mu(\mathrm{e})$ and form sets of lines which intersect at the transition energies between one preferred charge state and another (e.g. +2/+1). The lowest energies are shown as full lines from which it is seen that only the +2 charge state and the neutral state are preferred, both in the bulk and in the

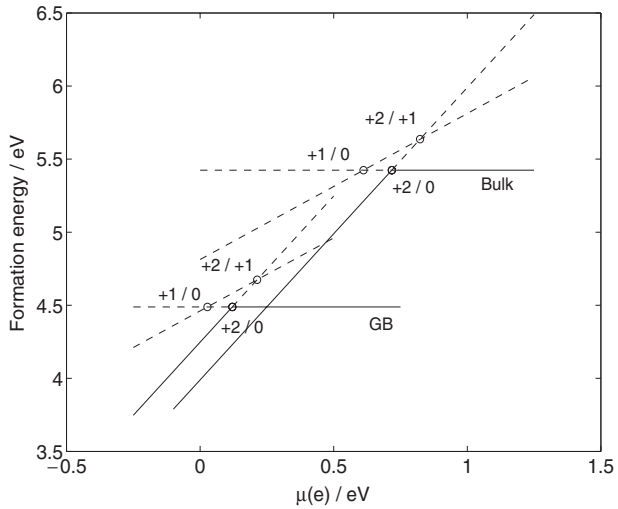

Figure 4. The formation energy of the oxygen vacancy as a function of electron chemical potential μ(e) for the 39-atom bulk and 119-atom GB systems. μ(e) = 0 refers to the energy of the highest occupied Kohn–Sham eigenstate.

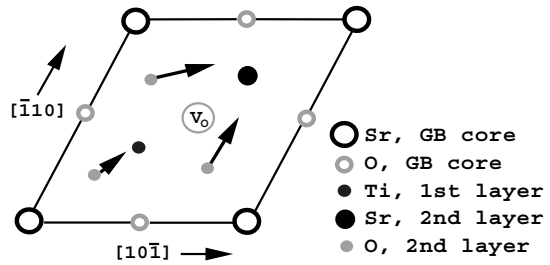

Figure 5. A plan view of the (111) GB plane with the neighbouring Ti and Sr–O planes projected onto it. The oxygen vacancy is labelled (V_O) and the arrows indicate schematically the relaxations of the oxygen atoms in the Sr–O plane.

GB. The +1 charge state is clearly unstable. The energy diagram consists of three regions. In the low-electron-chemical-potential region, corresponding to strongly p-type conditions (μ(e) < 0.1 eV), the oxygen vacancy prefers to donate two electrons into the bulk conduction band and thus become +2 charged. The energy of the +2 charged vacancy is lower in the bulk than in the GB and thus there is no driving force for segregation. When the electron chemical potential increases, the GB vacancy prefers to attract electrons from the bulk and become neutral. The neutral GB vacancy is energetically preferred (μ(e) > 0.2 eV) over the +2 charged bulk vacancy and there is a driving force for segregation which becomes stronger as the electron chemical potential increases. Finally, when the electron chemical potential region increases beyond $\mu = 0.7$ eV, both the bulk and GB vacancies are neutral and the strong preference for segregation continues. Since only the neutral vacancy binds to the GB the following discussion focuses on its properties rather than the properties of the charged vacancy.

The displacements induced by the charge neutral oxygen vacancy in the GB were found to be relatively small and confined to the two (111) layers on either side of the boundary plane.

In the 59-atom model, the Ti atoms nearest to the boundary moved outwards by 0.11 Å compared with their position in the stoichiometric structure. In the Sr–O planes nearest to the boundary the oxygen atoms underwent the largest relaxations. All oxygen atoms in these planes relax inwards towards the vacant site as shown schematically in figure 5. The magnitude of these displacements ranged from 0.06 Å for the oxygen atom furthest away from the vacancy to 0.22 Å for the two oxygen atoms closest to the vacancy.

The relaxations near the vacancy in the 119-atom model were similar to those in the 59-atom model. A small outwards expansion of the Ti plane nearest the non-stoichiometric boundary was present and the Ti atom nearest to the vacancy relaxed the furthest by 0.3 Å. Three of the four Sr atoms in the GB plane relaxed slightly (0.17–0.21 Å) away from the vacant site. The dissociation of the nearest Sr–O plane was again present, the magnitude of which was about 0.2–0.3 Å, and the Sr atoms were closer to the boundary than the oxygen atoms. The Sr atoms nearest to the vacancy in this plane behaved differently from the rest as they relaxed 0.2 Å further away from the GB. The two O atoms nearest to the vacancy in this plane had similar but smaller (0.14 Å) relaxations as was the case in the 59-atom model. The calculation on the 59-atom model indicated that most of the relaxations took place near the GB core and the same conclusion can be reached for the vacancy in the 119-atom model.

The electronic properties of the charge neutral oxygen vacancy in the GB were examined using the 59-atom model by evaluating the PDOS and by performing a Mulliken population analysis. Examination of the PDOS, which is shown in figure 6, indicates that the oxygen vacancy causes the lowest conduction levels to become occupied and that these levels originate from Ti d states which are partially hybridized with O p states. Most of the spin polarization was found to be localized on the Ti atoms in the bulklike region of the model and near the second defect-free GB. Some interesting behaviour was also observed in the Ti–O bonding next to the vacancy. The overlap population of the Ti–O bond opposite the vacant site increased to 0.73 implying a significant increase in covalency and the Mulliken charge on the oxygen atom decreased from -0.86 to -0.81 e. In contrast to this, the overlap population for the other Ti–O bond connected to that atom decreased to 0.30. The remainder of the Ti–O bonds in the boundary had overlap populations in the range 0.39–0.62 which is spread around the bulk value of 0.52. Most of the Mulliken charges were found to be close to those of the stoichiometric boundary model as shown in table 2. Small increases in the valence charge were observed near the GB containing the vacancy and also in the defect-free boundary in the model.

To further understand the effect of the oxygen vacancy on the electronic properties of the GB, the electrostatic potential across the supercell normal to the boundary plane was evaluated for the 59-atom model. The potential was averaged over each (111) plane in the cell and the results for the stoichiometric boundary and the boundary containing a vacancy are shown in figure 7. It is seen that the potential across the cell containing the stoichiometric boundary exhibits small oscillations but is roughly constant. The peaks in the oscillations coincide with the planes of positively charged Ti ions in the model. On the other hand, the potential near the non-stoichiometric GB becomes large and positive and this is compensated by a negative potential in the bulklike region of the model and in the second stoichiometric GB. This result indicates the formation of an electrostatic potential barrier at the boundary with an oxygen vacancy. The potential barrier can be interpreted as coming from a layer of ions with positive net charge which is then screened in the bulk part of the crystal. The formation of a potential barrier by a positively charged boundary which leads to surrounding space charge layers and pnp-type behaviour was suggested by Kim *et al* [20] in their study of a [001] tilt boundary in $SrTiO_3$. The result observed here is similar to this and the Mulliken charge analysis indicates the accumulation of a small amount of valence charge near the non-stoichiometric GB. In figure 7 are also plotted the electrostatic potentials for the 29- and 39-atom systems. Whilst

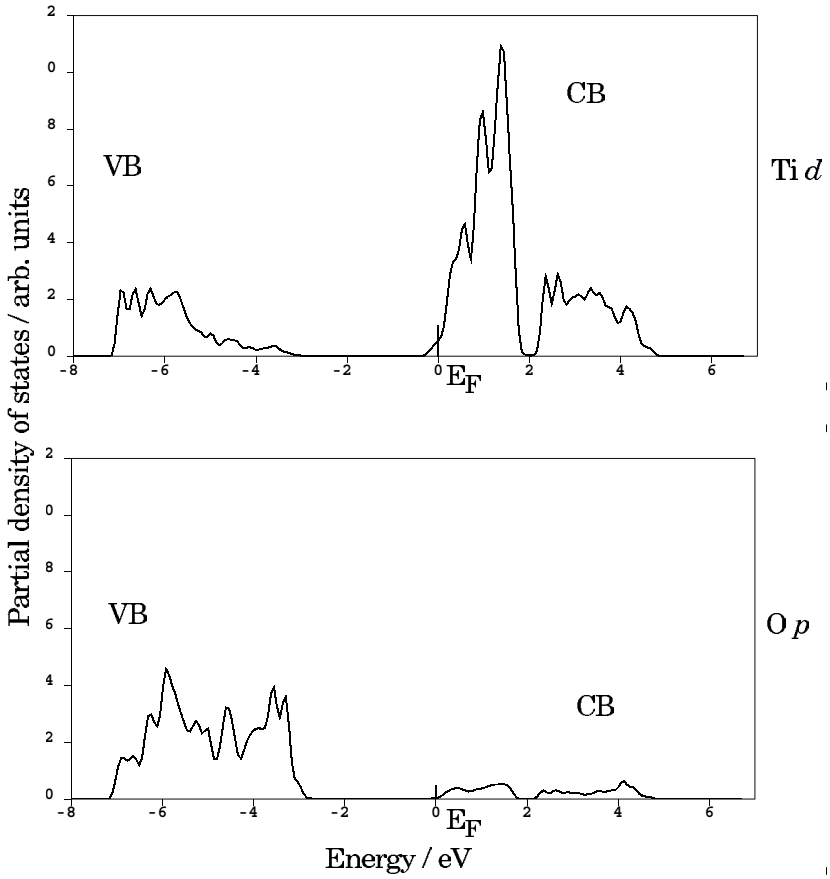

Figure 6. The PDOS for the GB containing an oxygen vacancy. For simplicity, only the d states on the Ti atom adjacent to the boundary plane are shown together with the p states on the O atom in the boundary plane. CB and VB denote the conduction and valence bands respectively.

the 29-atom system is too small to fully contain the barrier, it is seen that in the 39- and 59-atom systems the overall shape and height of the barrier are very similar. Therefore barrier formation is not significantly affected by size effects due to the presence of another GB in the supercell. However, care must be taken when attempting to generalize this result to more realistic systems containing impurities, as will be discussed in the next section.

4. Discussion and conclusions

The microscopic properties of an oxygen deficient $\Sigma = 3$ (111) [10$\bar{1}$] GB in $SrTiO_3$ have been investigated using *ab initio* computational methods. Except in p-type conditions, the GB was found to act as a sink for the oxygen vacancy since the formation energy of the point defect was lower in the boundary than in the bulk. The difference in energy was found to depend on the electron chemical potential. The atomic relaxations around the vacancy were small (typically <0.5 Å) and mainly confined to the neighbouring oxygen atoms. Previous calculations have indicated that the bulk oxygen vacancy acts as an effective donor [9]. At the GB the neutral vacancy is preferred since there is no driving force for segregation of the

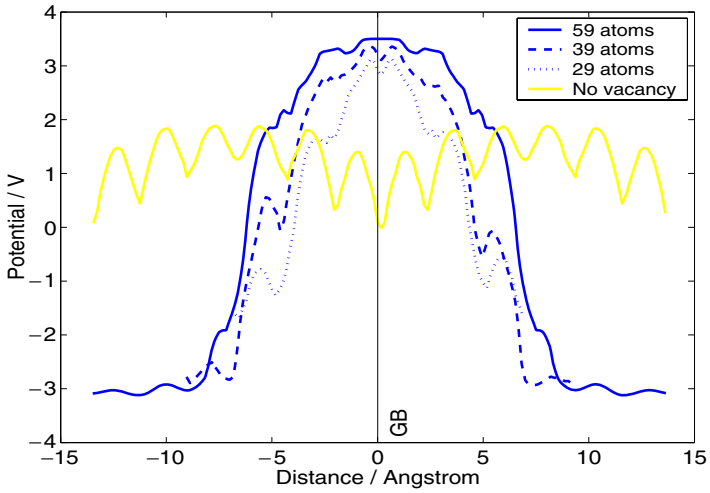

Figure 7. The electrostatic potential across four different GB supercells normal to the boundary plane. The potential was averaged over each (111) plane in the cell and presented as a function of distance from the GB plane. All the supercells, except the one without a vacancy, show a potential barrier. Note that because of the periodic boundary conditions, two GBs are present in each cell, one in the centre and one at the end. A positive potential indicates an increase in energy for a positive test particle. The potential is defined only up to an arbitrary constant.

(This figure is in colour only in the electronic version)

+2 charged vacancy. For the neutral vacancy the lowest hybridized Ti d–O p conduction levels become occupied. The formation of an electrostatic potential barrier at the non-stoichiometric GB was also observed.

There have been no direct experimental observations to suggest that oxygen vacancies may be present in the $\Sigma = 3$ (111) GB. However, to date, the boundary has only been studied using HRTEM which is not very sensitive to the presence of oxygen. Electron energy-loss spectroscopy would be a better tool for detecting oxygen at the interface as has been demonstrated for other GBs in $SrTiO_3$ [20]. Hitherto it has been assumed that the high degree of order present in the $\Sigma = 3$ boundary would not make it susceptible to vacancy (or impurity) segregation. The present calculations show that the oxygen vacancy in otherwise pristine material is attracted to this boundary and can form a potential barrier. However, the following points should be emphasized. The model studied here is highly simplified. In a real crystal there would be acceptor species present which are likely to segregate to the GBs. Oxygen vacancies lead to under-coordinated Ti ions and therefore their presence in the GB may further encourage the segregation of acceptors to these sites. It is therefore unclear whether the GB in a realistic bulk environment would be n- or p-type. However, the present results do suggest that oxygen vacancy segregation to $\Sigma = 3$ (111) GBs in polycrystalline $SrTiO_3$ could affect the electrical conductivity of the material. The undoped boundary becomes n-type by attracting oxygen vacancies. This behaviour can be understood by observing that the GB core is highly bulklike except for the Ti–O bonds and that the oxygen atoms in the boundary are weakly bound to their lattice sites. The formation of an electrostatic barrier is consistent with n-type behaviour for undoped oxygen deficient GBs. Further studies are required to investigate the behaviour of the oxygen vacancies in more general environments such as doped and more disordered GBs.

Acknowledgments

This work has been funded by EPSRC and the Finnish Academy of Sciences—Väisälä Foundation. Most of the calculations were performed at the Cambridge University High Performance Computing Facility.

References

[1] Beals M D 1970 *Refractory Materials, Volume 5-II: High Temperature Oxides* ed A M Alper (New York: Academic)
[2] Mauczok R and Wernicke R 1983/84 *Philips Tech. Rev.* **41** 338
[3] Aoki H, Hashimoto T, Ikawa E, Kikkawa T, Takeuchi K, Yamamichi S, Sakuma T and Miyasaka Y 1993 *Japan. J. Appl. Phys.* **32** 376
[4] Chambers S A, Liang Y, Yu Z, Droopad R and Ramdani J 2001 *J. Vac. Sci. Technol.* A **19** 934
[5] Eror N G and Balachandran U 1982 *J. Am. Ceram. Soc.* **65** 427
[6] Akhtar M J, Akhtar Z, Jackson R A and Catlow C R A 1995 *J. Am. Ceram. Soc.* **78** 421
[7] Crawford J and Jacobs P 1999 *J. Solid State Chem.* **144** 423
[8] Astala R and Bristowe P D 2001 *Comput. Mater. Sci.* **22** 81
[9] Astala R and Bristowe P D 2001 *Modelling Simul. Mater. Sci. Eng.* **9** 415
[10] Shanthi N and Sharma D D 1998 *Phys. Rev.* B **57** 2153
[11] Browning N D and Pennycook S J 1996 *J. Phys. D: Appl. Phys.* **29** 1779
[12] Browning N D, Buban J P, Moltaji H O, Pennycook S J, Duscher G, Johnson K D, Rodrigues R P and Dravid V P 1999 *Appl. Phys. Lett.* **74** 2638
[13] Chang H, Rodrigues R P, Xu J-H, Ellis D E and Dravid V P 1997 *Ferroelectrics* **194** 249
[14] Ravikumar V, Rodrigues R P and Dravid V P 1996 *J. Phys. D: Appl. Phys.* **29** 1799
[15] Ravikumar V and Dravid V P 1993 *Ultramicroscopy* **52** 557
[16] Johnson K D and Dravid V P 1999 *Appl. Phys. Lett.* **74** 621
[17] Hwang J-H, Johnson K D, Mason T O and Dravid V P 2000 *Appl. Phys. Lett.* **76** 2621
[18] Rodrigues R P, Chang H, Ellis D E and Dravid V P 1999 *J. Am. Ceram. Soc.* **82** 2385
[19] Rodrigues R P, Ellis D E and Dravid V P 1999 *J. Am. Ceram. Soc.* **82** 2395
[20] Kim M, Duscher G, Browning N, Sohlberg K, Pantelides S T and Pennycook S J 2001 *Phys. Rev. Lett.* **86** 4056
[21] Mo S-D, Ching W Y, Chisholm M F and Duscher G 1999 *Phys. Rev.* B **60** 2416
[22] Kienzle O, Exner M and Ernst F 1998 *Phys. Status Solidi* **166** 57
[23] Hutt S, Köstlmeier S and Elsässer C 2001 *J. Phys.: Condens. Matter* **13** 3949
[24] Geng W T, Zhao Y-J, Freeman A J and Delley B 2000 *Phys. Rev.* B **63** 060101(R)
[25] Makov G and Payne M C 1995 *Phys. Rev.* B **51** 4014
[26] Shah R 1996 *PhD Thesis* University of Cambridge ch 4
[27] Hagen M and Finnis M W 1998 *Phil. Mag.* A **77** 447
[28] Payne M C, Teter M P, Allan D C, Arias T A and Joannopoulos J D 1992 *Rev. Mod. Phys.* **64** 1045
[29] Vanderbilt D 1990 *Phys. Rev.* B **41** 7892
[30] Press W H, Flannery B P, Teukolsky S A and Vetterling W T 1989 *Numerical Recipes* (Cambridge: Cambridge University Press)
[31] Monkhorst H J and Pack J D 1974 *Phys. Rev.* B **13** 5188–92
[32] Segall M D, Pickard C J, Shah R and Payne M C 1996 *Mol. Phys.* **89** 571
[33] Segall M D, Shah R, Pickard C J and Payne M C 1996 *Phys. Rev.* B **54** 16 317–20
[34] Reihl B, Bednorz J G, Müller K A, Jugnet Y, Landgren G and Morar J F 1984 *Phys. Rev.* B **30** 803